Supporting Information

# Metal-Oxide Heterointerface Synergistic Effects of Copper-Zinc Systems for Highly Selective $CO_2$-to-$CH_4$ Electrochemical Conversion

*Xingcheng Ma[a], Dongxu Jiao[a], Jinchang Fan[a], Yilong Dong[a] and Xiaoqiang Cui[*a]*

a. State Key Laboratory of Automotive Simulation and Control, Key Laboratory of Automobile Materials of MOE and School of Materials Science and Engineering, Jilin University, Changchun, 130012, People's Republic of China.

Corresponding Author: Prof. Xiaoqiang Cui

E-mail: xqcui@jlu.edu.cn (X. Q. Cui)

## Experiments

### Materials and reagents

Copper nitrate and zinc nitrate was obtained from Sinopharm Chemical Reagent, China. Copper powder (200 mesh) was purchased from Sinopharm Chemical Reagent, China. Tissue paper was produced by Hengan International Group Co. Ltd. Potassium bicarbonate (99.95%) was obtained from Sigma-Aldrich Co., Ltd. Ethanol (AR) was purchased from Sinopharm Chemical Reagent, China. High-purity carbon dioxide (99.995%) was obtained from Dalian Special Gases Co., Ltd, China. High-purity argon was obtained from Xin'guang Gas Co., China. The deionized water (18.2 $M\Omega$ cm) used in all experiments was prepared using an ultrapure purification system. All reagents were used as received without further purification.

### Characterization

Scanning electron microscope (SEM) images were obtained with a Hitachi SU8010 with a 30 kV accelerating voltage. Transmission electron microscope (TEM) and high-resolution transmission electron microscope (HRTEM) studies were conducted on JEM-2100F (JEOL Co., Japan). X-ray photoelectron spectroscopy (XPS) data was acquired with an ESCALAB-250 from Thermo Fisher Scientific, USA. This used an Al-K$\alpha$ (1486.6 eV) radiation source and a 0.1 eV hemisphere detector. X-Ray diffraction (XRD) patterns were acquired using a Bragg-Brentano diffractometer (D8-tools, Germany) with a Cu-K$\alpha$ line source at 0.15418 nm. Ultrasonic cleaning was done with a frequency of 40 kHz at 800 W (KQ-800KDE, Kunshan Ultrasonic Instrument Co. Ltd.).

**Electrochemical characterizations and product analysis**

Electrocatalytic measurements were tested in a two-compartment gas-tight electrochemical H-cell with a piece of Nafion 117 (proton exchange membrane). The working electrode was prepared by loading 0.3 mL of 5 mg / mL catalyst and 6 μL nafion onto a carbon paper electrode (1 cm × 1.5 cm). A platinum foil (2 cm×2 cm) and an Ag / AgCl (in saturated KCl solution) electrode were used as the counter and reference electrodes, respectively. All the potentials were calibrated to a reversible hydrogen electrode ($E_{RHE} = E_{Ag/AgCl} + 0.0591$ V × pH +0.197 V). The electrode was electrochemical activated in a $CO_2$-saturated 0.1 M $KHCO_3$ solution by performing cyclic voltammetry scanning at -0.4 V to -1.1 V vs. RHE for 10 cycles with a scan rate of 20 mV / s by CHI 760E before each electrochemical test. Linear sweep voltammetry (LSV) was done in 0.1 M $KHCO_3$ solution (saturated with $CO_2$) between -0.4 V and -1.1 V vs. RHE with a scan rate of 20 mV / s. Long-term stability was tested by taking a chronoamperometric curve. All data are presented without i-R compensation.

$CO_2$ reduction products were measured by gas chromatography (Shimadzu, GC2014) and nuclear magnetic resonance (NMR, Bruker 600 MHz), for the gas and liquid products, respectively. Both instruments were calibrated with standard gases or liquid solutions. The outlet of the cathode compartment was connected to the GC inlet for real time gas phase product analysis. Automatic valve injection (1 mL sample) with a thermal conductivity detector (TCD) and flame ionization detector (FID) were used in the GC system. Ultrahigh purity argon was used as the carrier gas for all experiments. High purity $CO_2$ was

continuously flowed into the gas-tight H-cell during the electrochemical test. A flow rate of 20 SCCM was used. For Faradaic efficiency (*FE*) analysis, the gas products were detected by using the online gas chromatography. Gas samples could be taken every 15 minutes.

**First principles calculations**

All the spin-polarized DFT calculations were performed by using the Vienna Ab Initio Simulation Package (VASP) [1, 2], in which the electrons and ions interactions were described by the projector augmented wave (PAW) potential [3, 4]. The exchange-correlation interactions were treated using generalized gradient approximation (GGA) combined with Perdew, Burke, Ernzerhof (PBE) functional [5]. All these computations in this work were carried out by using a plane wave energy cutoff of 500 eV, and the convergence criterion for the residual force and energy was set to 0.05 eV $\text{Å}^{-1}$ and $10^{-5}$ eV, respectively. The empirical correction was used to describe the van der Waals (vdW) interactions by Grimme's scheme (DFT+D3) method [6].

In our computation, for the Cu-ZnO model, we used a supercell comprising $3 \times 3$ Cu (111) and $2 \times 2$ ZnO (002) cells. During the geometrical optimization, the bottom two layers of Cu(111) and the top two layers of ZnO (002) were fixed, while the remaining atoms were relaxed. The k-points were set to $3 \times 3 \times 1$ with the Monkhorst-Pack mesh was utilized for all the computations. The adsorption energy ($E_{\text{ads}}$) of the adsorbate on the surface was defined as: $E_{\text{ads}} = E_{\text{total}} - E_{\text{adsorbate}} - E_{\text{surface}}$, in which the $E_{\text{total}}$, $E_{\text{adsorbate}}$, and $E_{\text{surface}}$ represent the total energy of the adsorbed species on the surface, the isolated adsorbate, and the pristine surface, respectively. Furthermore, the thermodynamic free energies of each elementary step in the whole $CO_2ER$ process were determined by the computational hydrogen electrode (CHE) technique proposed by Nørskov *et al* [7, 8]. According to this model, the changes in Gibbs free

4

energy ($\Delta G$) for all electrochemical steps was defined as: $\Delta G = \Delta E + \Delta E_{ZPE} - T\Delta S + \Delta G_{pH}$, where the reaction energy ($\Delta E$) can be directly obtained by analyzing the DFT total energies. The zero-point energy difference ($\Delta E_{ZPE}$) between the products and the reactants can be computed from the vibrational frequencies. $\Delta S$ is the change in entropy between the products and the reactants at room temperature (T = 298.15 K). $\Delta G_{pH}$ was the free energy contribution due to the variations in H concentration, which can be determined as: $\Delta G_{pH} = 2.303 \times k_B T \times$ pH, where the value of pH was set to 0 in calculation.
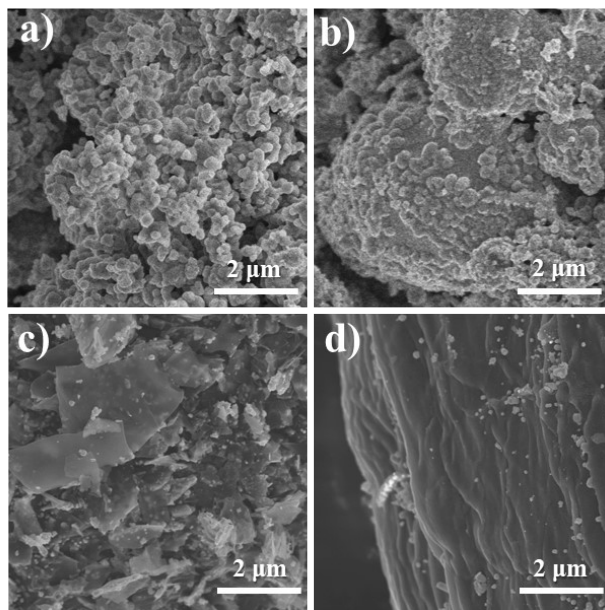
**Figures**
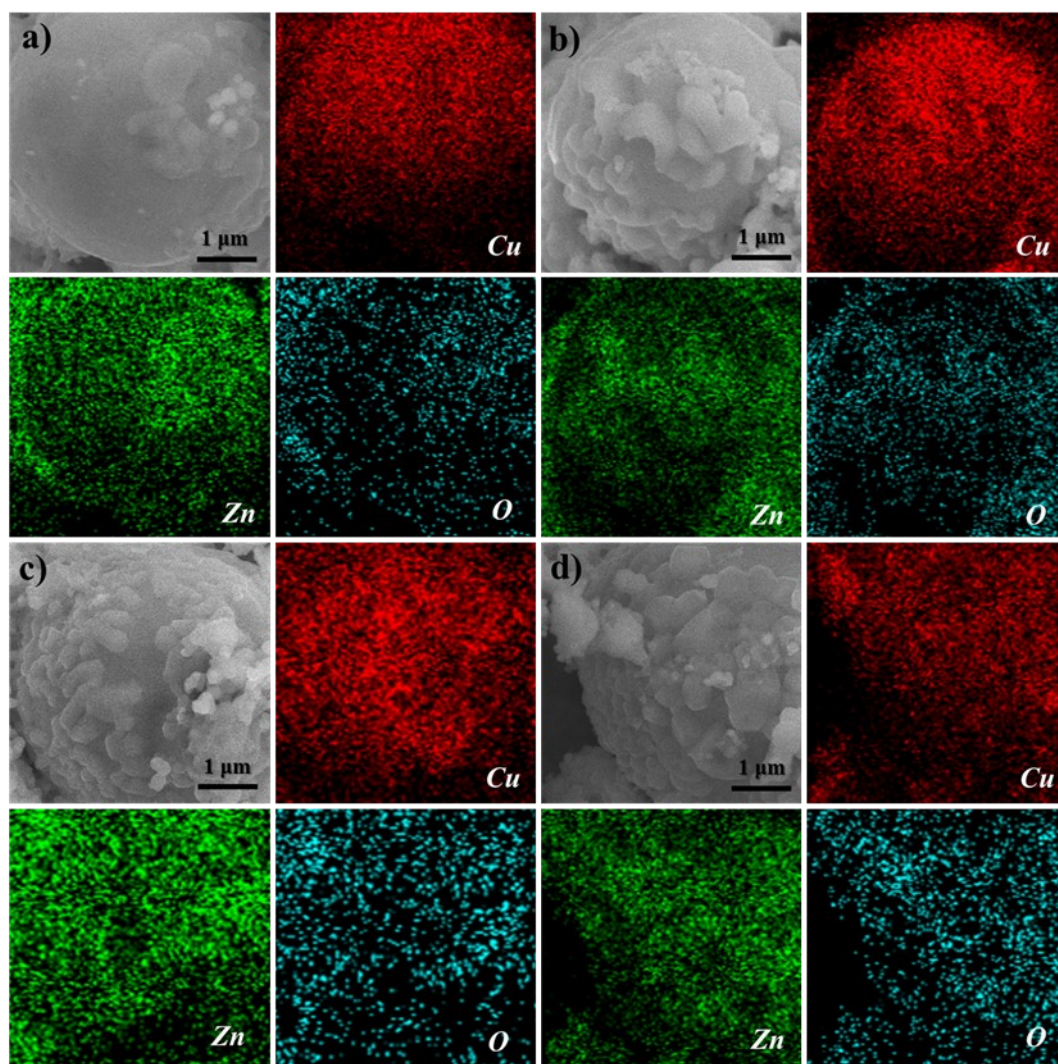


**Figure S1.** SEM-mapping images of a) 9Cu-1ZnO/C, b) 4Cu-1ZnO/C, c) 2Cu-1ZnO/C
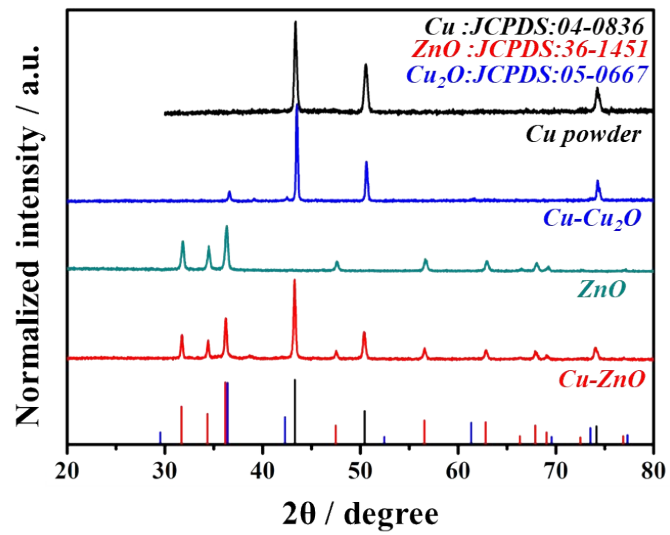
and d) 1Cu-1ZnO/C.
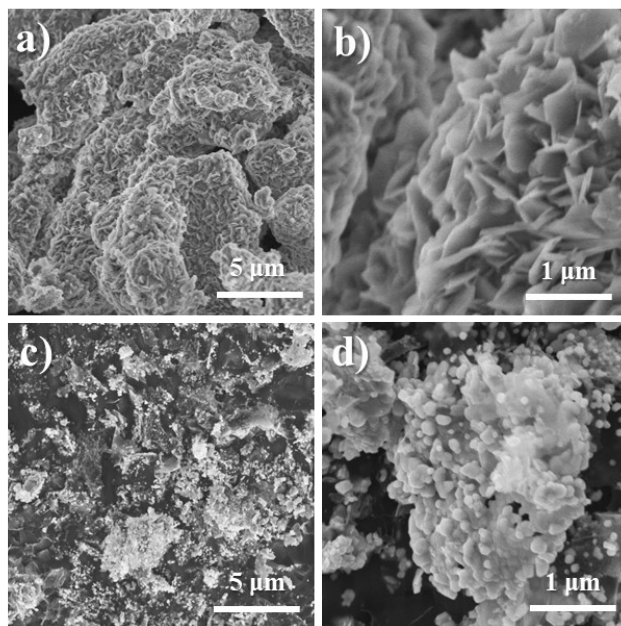
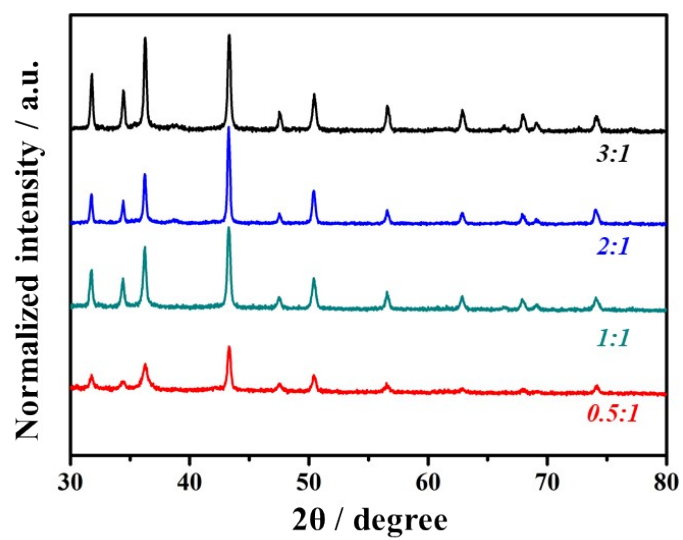**Figure S2.** SEM images of a-b) Cu-Cu$_2$O and c-d) ZnO.

**Figure S3.** SEM images of different Cu+Zn: tissue paper feed ratios: a) 3:1, b) 2:1, c) 1:1 and d) 1:2.
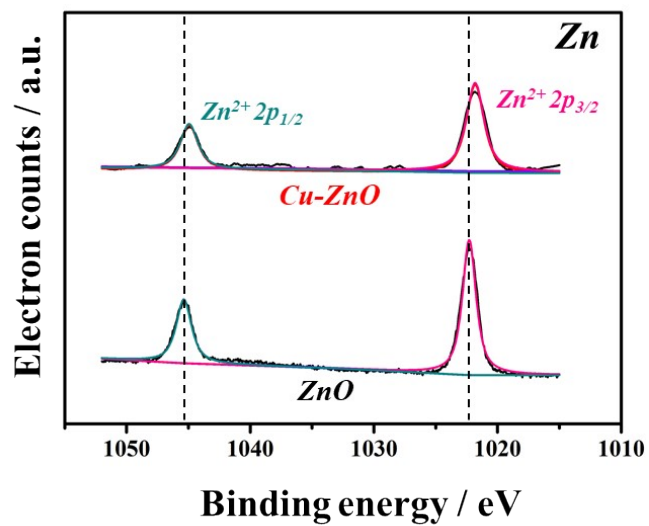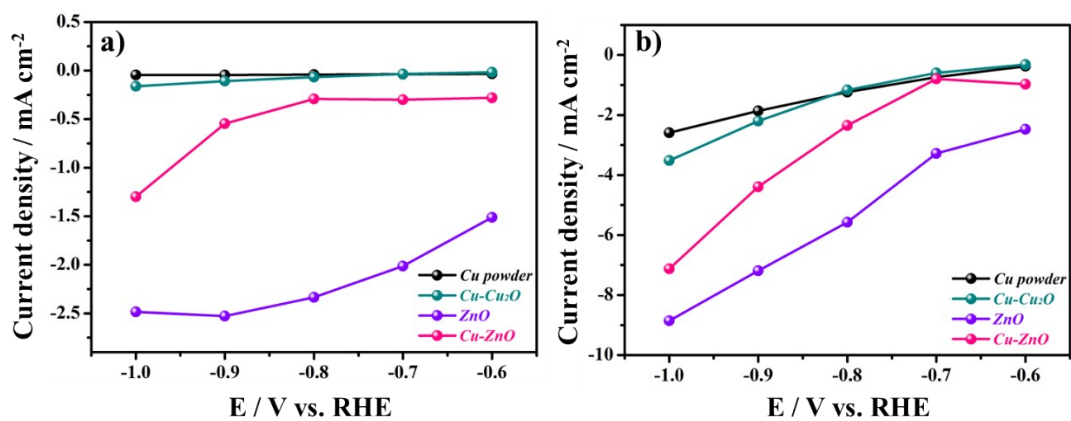
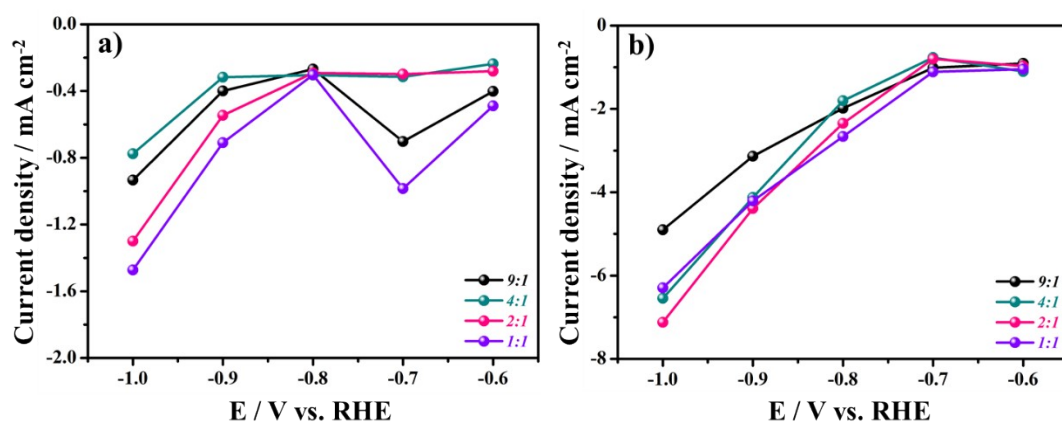**Figure S4.** XRD patterns of Cu powder, Cu-Cu$_2$O, ZnO and Cu-ZnO.

**Figure S5.** XRD patterns of Cu-ZnO catalysts with different Cu+Zn: tissue paper feed
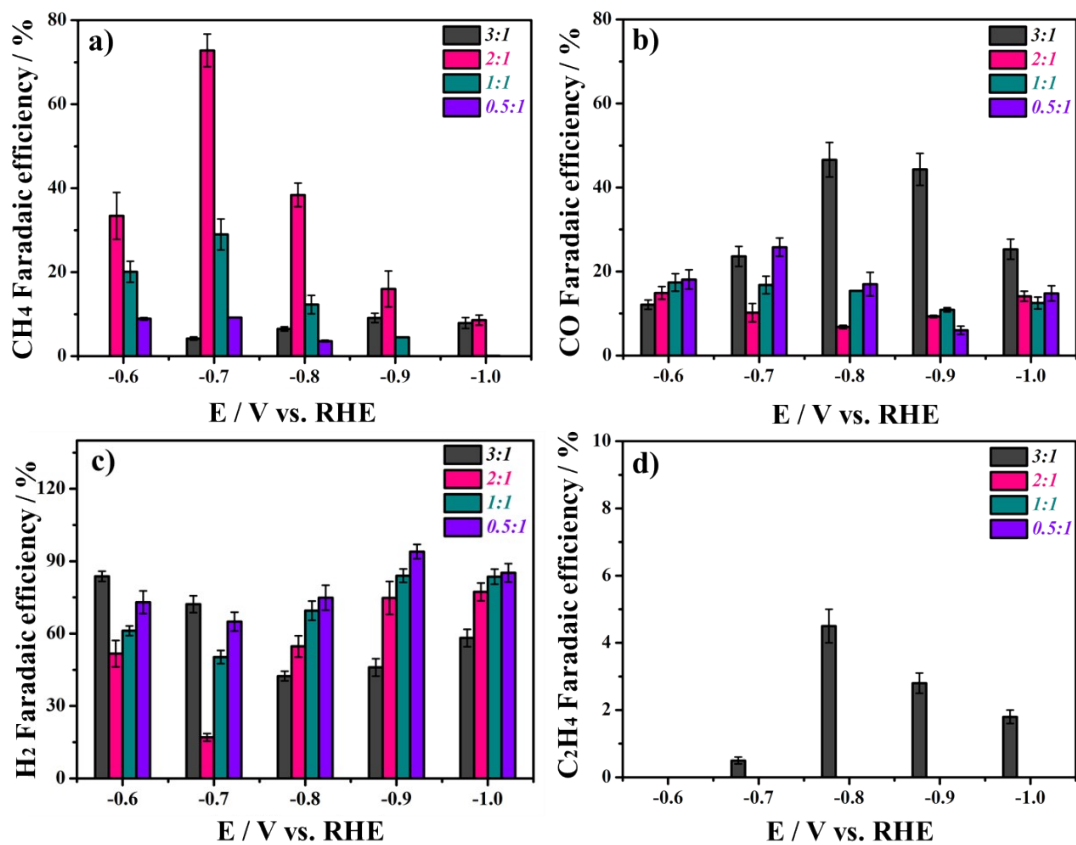
ratios.

**Figure S6.** High-resolution XPS of 2Cu-1ZnO and ZnO.

**Figure S7.** a) CO and b) $H_2$ partial current density of Cu powder, Cu-$Cu_2$O, ZnO and Cu-ZnO catalysts.
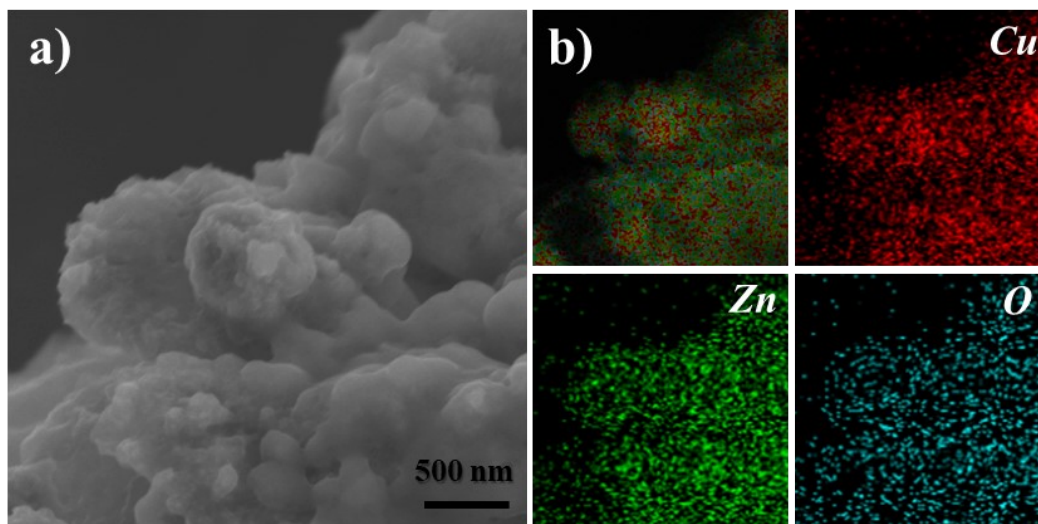
**Figure S8.** a) CO and b) H$_2$ partial current density of Cu-ZnO catalysts with different Cu:Zn ratios.

**Figure S9.** a) CH$_4$ faradaic efficiency, b) CO faradaic efficiency, c) H$_2$ faradaic efficiency and d) C$_2$H$_4$ faradaic efficiency of Cu-ZnO catalysts with different Cu+Zn: tissue paper feed ratios.
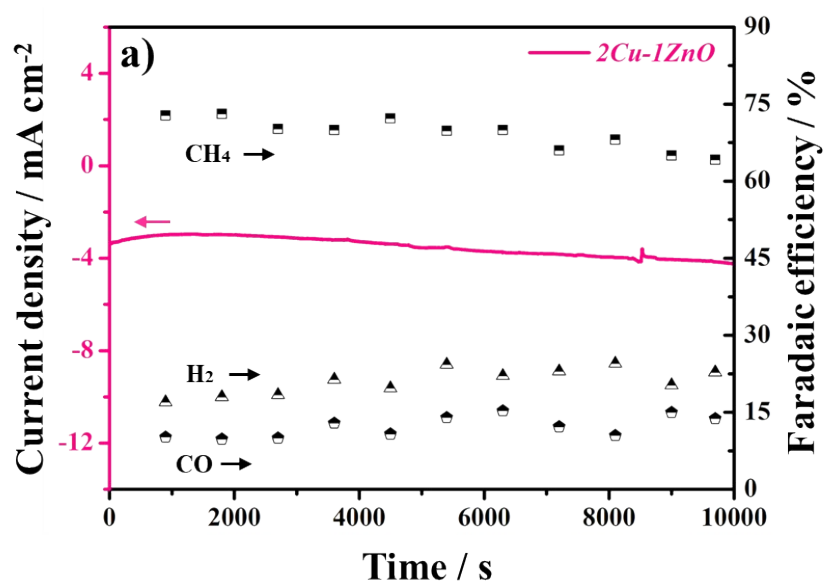
**Figure S10.** I-t test of 2Cu-1ZnO. The catalyst exhibits good stability.

**Figure S11.** a) SEM and b) SEM-mapping images of 2Cu-1ZnO after the electrochemical test. Zn and O were in similiar distribution and Cu exhibited complenentary patterns.
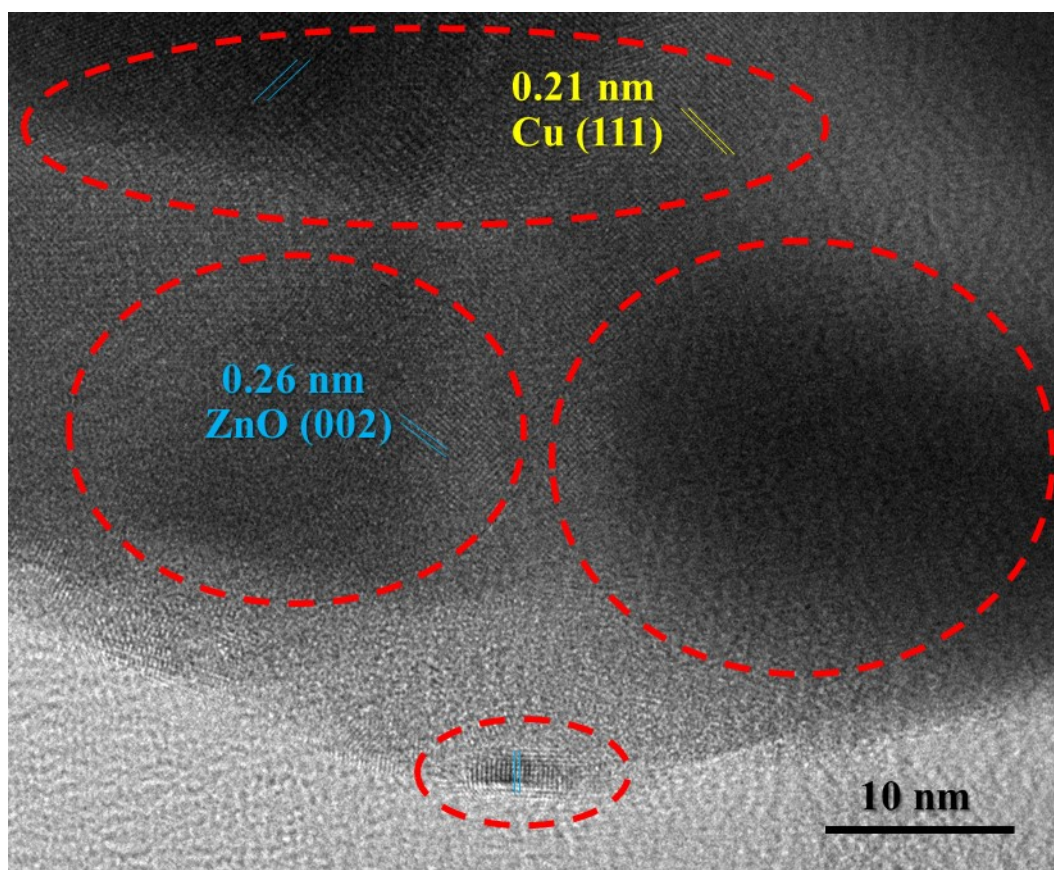
**Figure S12.** TEM image of 2Cu-1ZnO after the electrochemical test. It is clear to see heterointerfaces in red circles.
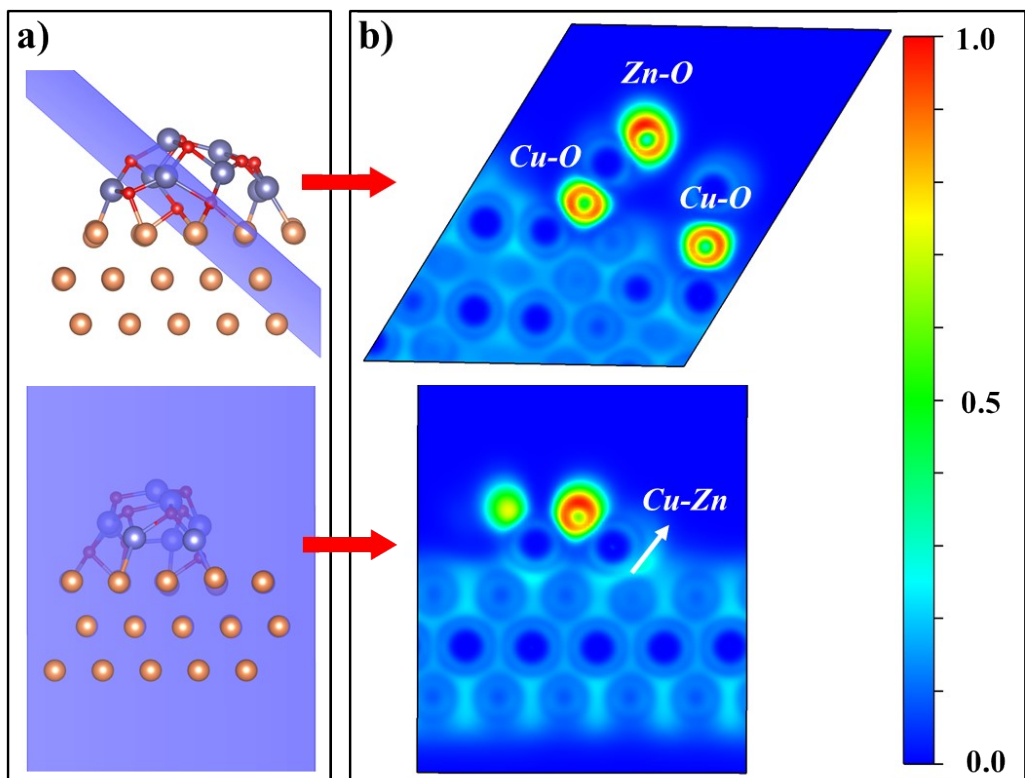
**Figure S13.** a) The stable structure and b) sliced electron localization function (ELF) maps of the 2Cu-1ZnO catalyst.

**Figure S14.** The energy barrier of the formation of $H_2$ for Cu-ZnO system following the Volmer-Tafel mechanism.

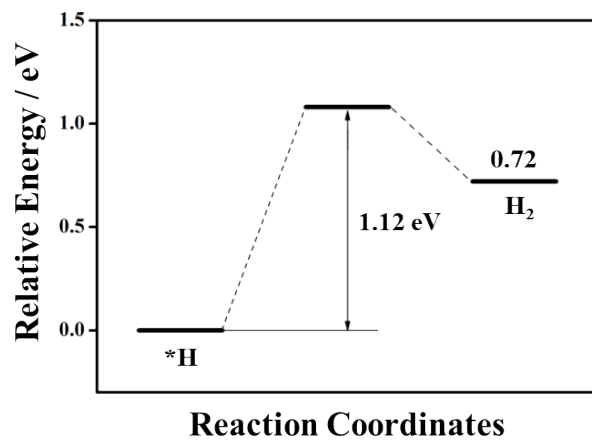| Materials | Potential ($V_{RHE}$) | main product | FE | Reference |
|---|---|---|---|---|
| Cu-ZnO | -0.7 | $CH_4$ | 72.8% | This work |
| CuZn0.4 | -1 | CO | 70% | 9 |
| CuO/ZnO/C | -0.75 | $C_2H_4$ | 50.9% | 10 |
| ZnO | -1 | CO | 30% | 11 |
| Cu oxides/ZnO | -1.9 | $C_2H_4$ | 91.1% | 12 |
| $Cu_2O$/ZnO | -0.65 | $CH_3OH$ | 17.7% | 13 |
| GN/ZnO/$Cu_2O$ | -0.25 | $C_3H_7OH$ | 30% | 14 |
| ZnO/CuO | -1.15 | $C_2H_5OH$ | 32% | 15 |
| ZnO nanosheet | -1.1 | CO | 83% | 16 |

**Table S1.** A comparison of this work with other ZnO-based materials previously reported data.

| Materials | Potential ($V_{RHE}$) | r ($\mu mol\,m^{-2}s^{-1}$) | FE | Reference |
|---|---|---|---|---|
| Cu-ZnO | -0.7 | 5.78 | 72.8% | This work |
| Cu oxides/ZnO | -1.9 | 3.5 | <1% | [12] |
| Cu 60-80 nm | -1.1 | 4.1 | 2.0% | [17] |
| Cu 40-60 nm | -1.9 | 4.23 | 1.1% | [17] |
| Cu 25 nm | -1.6 | 37.6 | 4.17% | [17] |
| Cu NPs | -1.4 | 4.40 | 4.5% | [18] |
| Cu foil | -1 | 10 | 60% | [19] |

**Table S2.** A comparison of the present system with other Cu-based materials applied in the literature for $CO_2$ electroreduction to $CH_4$.

# Reference

1    G. Kresse and J. Hafner, Ab initio molecular dynamics for liquid metals, *Phys. Rev. B*, 1993, **47**, 558-561.

2    G. Kresse and F. J., Efficient iterative schemes for ab initio total-energy calculations using a plane-wave basis set, *Phys. Rev. B*, 1996, **54**, 11169-11186.

3    P. E. Blochl, Projector augmented-wave method, *Phys. Rev. B*, 1994, **50**, 17953-17979.

4    G. Kresse. and D. Joubert., From ultrasoft pseudopotentials to the projector augmented-wave method, *Phys. Rev. B*, 1999, **59**, 1758-1775.

5    John P. Perdew, Kieron Burke and M. Ernzerhof., Generalized gradient approximation made simple, *Phys. Rev. Lett.*, 1996, **77**, 3865-3868.

6    S. Grimme, Semiempirical GGA-type density functional constructed with a long-range dispersion correction, *J. Comput. Chem.*, 2006, **27**, 1787-1799.

7    J. K. Nørskov, J. Rossmeisl, A. Logadottir and L. Lindqvist, A. Logadottir and L. Lindqvist, Origin of the overpotential for oxygen reduction at a fuel-cell cathode, *J. Phys. Chem. B*, 2004, **108**, 17886-17892.

8    A. A. Peterson, F. Abild-Pedersen, F. Studt, J. Rossmeisl and J. K. Nørskov, How copper catalyzes the electroreduction of carbon dioxide into hydrocarbon fuels, *Energy Environ. Sci.*, 2010, **3**, 1311.

9    J. Zeng, T. Rino, K. Bejtka, M. Castellino, A. Sacco, M. A. Farkhondehfal, A. Chiodoni, F. Drago and C. F. Pirri, Coupled copper-zinc catalysts for electrochemical reduction of carbon dioxide, *ChemSusChem*, 2020, **13**, 4128-4139.

10   Z. Li, R. M. Yadav, L. Sun, T. Zhang, J. Zhang, P. M. Ajayan and J. Wu, CuO/ZnO/C electrocatalysts for $CO_2$-to-$C_{2+}$ products conversion with high yield: on the effect of geometric structure and composition, *Appl. Catal., A*, 2020, **606**, 117829.

11   R. Daiyan, E. C. Lovell, B. Huang, M. Zubair, J. Leverett, Q. Zhang, S. Lim, J. Horlyck, J. Tang, X. Lu, K. Kalantar-Zadeh, J. N. Hart, N. M. Bedford and R. Amal, Uncovering atomic-scale stability and reactivity in engineered zinc oxide electrocatalysts for controllable syngas production, *Adv. Energy Mater.*, 2020, **10**, 2001381.

12   I. Merino-Garcia, J. Albo, J. Solla-Gullón, V. Montiel and A. Irabien, Cu oxide/ZnO-based surfaces for a selective ethylene production from gas-phase $CO_2$ electroconversion, *J. $CO_2$ Util.*, 2019, **31**, 135-142.

13   J. Albo, A. Sáez, J. Solla-Gullón, V. Montiel and A. Irabien, Production of methanol from $CO_2$ electroreduction at $Cu_2O$ and $Cu_2O$/ZnO-based electrodes in aqueous solution, *Appl. Catal., B*, 2015, **176-177**, 709-717.

14   R. A. Geioushy, M. M. Khaled, K. Alhooshani, A. S. Hakeem and A. Rinaldi, Graphene/ZnO/$Cu_2O$ electrocatalyst for selective conversion of $CO_2$ into n-propanol, *Electrochim. Acta*, 2017, **245**, 456-462.

15   D. Ren, J. Gao, L. Pan, Z. Wang, J. Luo, S. M. Zakeeruddin, A. Hagfeldt and M. Gratzel, Atomic layer deposition of ZnO on CuO enables selective and efficient electroreduction of carbon dioxide to liquid fuels, *Angew. Chem. Int. Ed.*, 2019, **58**, 15036-15040.

16   Z. Geng, X. Kong, W. Chen, H. Su, Y. Liu, F. Cai, G. Wang and J. Zeng, Oxygen vacancies in ZnO nanosheets enhance $CO_2$ electrochemical, *Angew. Chem. Int. Ed.*, 2018, **57**, 6054-6059.

17   I. Merino-Garcia, J. Albo and A. Irabien, Tailoring gas-phase $CO_2$ electroreduction selectivity to hydrocarbons at Cu nanoparticles, *Nanotechnology*, 2018, **29**, 014001.

18   I. Merino-Garcia, J. Albo and A. Irabien, Productivity and selectivity of gas-phase $CO_2$ electroreduction to methane at copper nanoparticle-based electrodes, *Energy Technol.*, 2017, **5**, 922-928.

19.  A. S. Varela, W. Ju, T. Reier and P. Strasser, Tuning the catalytic activity and selectivity of Cu for CO2 electroreduction in the presence of halides, *ACS Catal.*, 2016, **6**, 2136-2144.